Proceedings of the 17th World Congress
The International Federation of Automatic Control
Seoul, Korea, July 6-11, 2008

Intelligent Integrated Model for Predicting Burn-Through Point Based on Gas Temperature Distribution ⋆

Chen-Hua Xu [*,***] **Min Wu** [*] **Jin-Hua She** [**] **Lei Ding** [*]
Ryuichi Yokoyama [***]

[*] *School of Information Science and Engineering, Central South University, Changsha 410083, China*
[**] *School of Bionics, Tokyo University of Technology, Hachioji, Tokyo 192-0982, Japan*
[***] *Graduate School of Environment and Energy Engineering, Waseda University, Tokyo 169-0051, Japan*

Abstract: This paper presents an integrated model for predicting the burn-through point (BTP) of the lead-zinc sintering process from the gas temperature distribution (GTD). This process features strong nonlinearity, a large time delay, and time-varying parameters. First, the characteristics of the GTD in the sintering machine are obtained from experiments, and a surface temperature model for the material is established. Based on that model, the current BTP is obtained by a soft-sensing technique. Then, a time-sequence-based model for predicting the BTP is built using grey theory. Since the BTP is affected by variations in the process parameters, a technological-parameter-based prediction model of the BTP is set up using a neural network. Finally, an integrated model for predicting the BTP is implemented using a fuzzy classifier to integrate the time-sequence-based and technological-parameter-based models. The results of actual runs demonstrate the validity of the method.

1. INTRODUCTION

The lead-zinc sintering process (LZSP) aims at obtaining good permeability, producing sintering agglomerate with the appropriate composition, etc. Its features include strong nonlinearity, a large time delay, and time-varying parameters (Jak et al. [2003]). In practice, the burn-through point (BTP) is defined to be the position on the trolley with the highest temperature (Siemon et al. [1991]). It not only reflects the burning state of the material being sintered, but can also be regarded as a criterion for determining product quality and quantity. The complexity of the sintering process makes it difficult to measure the BTP on-line. So, it is necessary to construct a model that uses related measurement parameters to determine and predict the BTP so as to implement state optimization of the LZSP.

At present, the prediction and control of the BTP in the LZSP is usually handled by operators. The prediction of the BTP is influenced by various factors (characteristics of gas flow in the sintering machine, placement of thermocouples, etc.), which can lead to variations in the process state and incomplete sintering.

Intelligent techniques (neural networks (NNs), fuzzy theory, etc.) are now widely used for the modeling and control of complex systems (Li & Sun [2004], Terpak et al. [2005] and Yuan & He [2006]); and integrated modeling, which combines a model of the process mechanism with NNs, produces good results (Kwon et al. [1999], Joo et al. [2000], Wu et al. [2001] and Yang et al. [2002]). At the same time, these methods also provide a clue about how to determine and predict the BTP in the LZSP.

This paper presents an intelligent integrated model for predicting the BTP from the gas temperature distribution (GTD). First, the features of the GTD in a sintering machine are described by an NN; and a model of the surface temperature of the material is established. Next, this model in combination with a soft-sensing technique is used to obtain the current BTP. Then, a time-sequence-based model for predicting the BTP is built using grey theory. To deal with parameter variations, a technological-parameter-based model for predicting the BTP is also set up using an NN. To obtain high-accuracy predictions of the BTP, an integrated model for predicting the BTP is established that employs a fuzzy classifier to integrate the time-sequence-based and technological-parameter-based models. Finally, the results of actual runs show that the integrated model provides high precision and good adaptability.

2. SINTERING PROCESS AND FEATURE ANALYSIS

The blast sintering process (BSP) considered in this study employs a Dwight-Lloyd (DL) sintering machine (Fig. 1).

The materials are proportioned, blended, granulated, and formed into blended balls with the appropriate water content. A shuttle distributor sends the balls to the ignition

⋆ This work was supported by the National Science Fund for Distinguished Youth Scholars of China (60425310), and the National High Technology Research and Development Program of China (2006AA04Z172).
Corresponding author: min@csu.edu.cn (M. Wu)

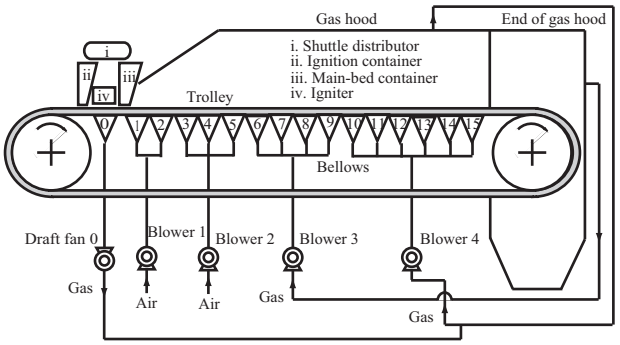

Fig. 1. Dwight-Lloyd sintering machine.

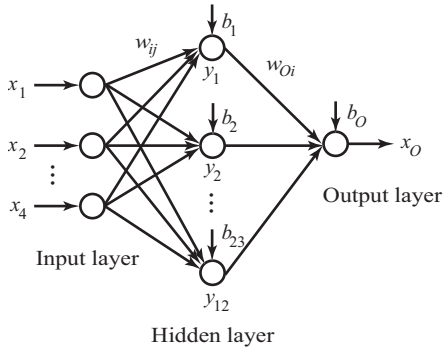

Fig. 2. Structure of BPNN.

container and main-bed container. Balls are poured onto a trolley to a depth of 3 cm to form a bed called the ignition layer and are ignited by the igniter. The ignition temperature is controlled by means of the gas flux. Once the ignition layer is burning, more balls are added on top to form a bed 30-40 cm thick. The trolley propels the material along. After four phases (evaporation, heating, reaction, sintering), the balls become sintering agglomerate with a certain structure, and are discharged from the end of the sintering machine. Good-quality agglomerate is sent to the smelting process while the rest goes through a two-level fragmentation and cooling process and is sent back to the beginning of the process as returned powder (Tang et al. [1992]).

In the LZSP, the BTP is a key factor in estimating the quality and quantity of product. If the BTP occurs too soon or too late, then the quantity of sinter decreases and the amount of returned powder increases.

The surface temperature of the material is the key parameter needed to determine the BTP. At present, it is estimated from the temperature of the gas above the material, as measured with thermocouples. Generally, thermocouples are placed above the bellows and below the top of the gas hood. However, many factors affect the flow of gas in the hood, which makes it difficult to obtain the exact temperature distribution just from measurements at a single distance below the top of the hood (e.g., 2.5 m). On the other hand, the surface of the material is about 3.6 m below the top of the hood. So, the temperature measured at 2.5 m does not accurately reflect the actual surface temperature of the material. In the measurement process, the closer a thermocouple is to the surface of the material, the closer the measured temperature is to the temperature of that surface; and there exists a certain regularity in the GTD that reflects the change in gas temperature with distance. This study investigated the GTD of the sintering machine of a nonferrous metal smeltery, and used it to predict the BTP of the LZSP.

3. MODEL OF GAS TEMPERATURE DISTRIBUTION

In this paper, we use the expression "hood distance" to mean the distance below the top of the gas hood. In actual production, usually only one thermocouple is installed above each bellows at a hood distance of 2.5 m. To avoid interfering with normal operations, temperature experiments were carried out at only one hood distance on Bellows 1 and 3, and Bellows 12-15. The rest of the bellows were divided into five groups: 2 & 4, 5 & 7, 6, 8 & 9, and 10 & 11. In order to obtain the GTD, a series of measurements was carried out on each group. First, the gas temperature at a hood distance of 2.5 m was measured. Then, for the target group, measurements were made at each of the hood distances 2.7 m, 2.9 m, and 3.1 m; while for the other bellows, measurements were made simultaneously at a hood distance of 2.5 m. NNs were built to describe the GTD above each bellows.

3.1 NN Models

To explain an NN model, we take the measurements for the group containing Bellows 2 and 4 as an example. A back propagation NN (BPNN) with a three-layer structure (4-12-1) is employed to build a fitted temperature model for each bellows in the group for a hood distance of 2.5 m, as shown in Fig. 2.

If we let $T_i(h)$ be the measured temperature of Bellows i at hood distance h, then for the inputs $T_i(2.5)$, $(i = 1, 3, 5, 6)$, we obtain the following BPNN model $(k = 2, 4)$:

$$\hat{T}_k(2.5) = x_O = \sum_{i=1}^{12} \omega_{Oi} \text{tansig}\left(\sum_{j=1}^{4} \omega_{ij} x_j + b_i\right) + b_O. \quad (1)$$

In this equation, for $i = 1, \cdots, 12$ and $j = 1, \cdots, 4$, ω_{ij} is the weight of the signal from the j-th neuron of the input layer to the i-th neuron of the hidden layer; b_i is the bias of the i-th neuron of the hidden layer; ω_{Oi} is the weight of the signal from the i-th neuron of the hidden layer to the neuron of the output layer; and b_O is the bias of the neuron of the output layer. The weights ω_{ij} and the biases b_i and b_O are determined by training the BPNN.

Table 1 shows gas temperatures measured at a particular time.

3.2 Training of Models

This section explains how a BP algorithm (Hagan et al. [2002]) is used to train the NNs. The performance function of the NNs is

Table 1. Gas temperature at measurement points (°C).

Measured gas temperature (°C)					
$T_1(2.5)$	$T_2(2.5)$	$T_3(2.5)$	$T_4(2.5)$	$T_5(2.5)$	$T_6(2.5)$
89	148	158	212	371	411

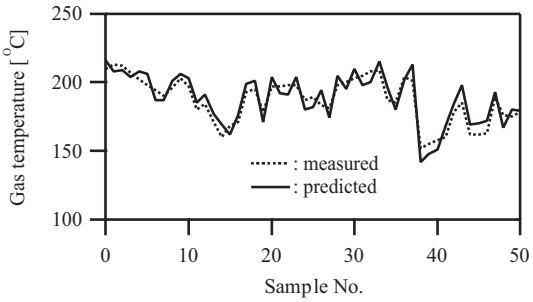

Fig. 3. Verification results for model for Bellows 2.

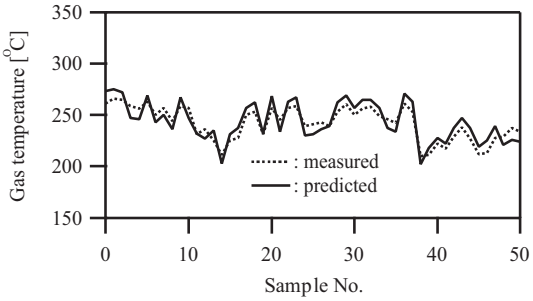

Fig. 4. Verification results for model for Bellows 4.

$$J = \frac{1}{N}\sum_{k=1}^{N}\left[x_O(k) - x_{OA}(k)\right]^2, \tag{2}$$

where N is the number of samples; and $x_O(k)$ and $x_{OA}(k)$ are the measured and predicted values, respectively, of the k-th sample. The goal of the training is to obtain the smallest value of J. The training used to determine the weights and biases is performed off-line. Whenever the state of the process changes, the weights and biases need to be relearned.

3.3 Verification of Models

1000 sets of qualified data were used for modeling and verification. The initial values of the weights and biases were always in the range $[-1, 1]$. Trial learning results showed the learning rate to be 0.2. Simulation results for fitted models are shown in Figs. 3 and 4.

An analysis of the data for the models for Bellows 2 and 4 shows that the average relative errors are 3.59% and 3.35%, respectively. These values easily satisfy the engineering requirement of an allowable error of 10%.

3.4 Features of Gas Temperature Distribution

We use the group containing Bellows 2 and 4 as an example to explain the characteristics of the GTD. For these two bellows, the gas temperatures were measured at four different hood distances (2.5 m, 2.7 m, 2.9 m, 3.1 m); while for the other bellows, measurements were made at only one hood distance, as shown in Fig. 5. The gas temperature at a hood distance of 2.5 m is taken to be the reference.

The measured gas temperatures for Bellows 2 and 4 are shown in Table 2. The data in each row were measured at the same time.

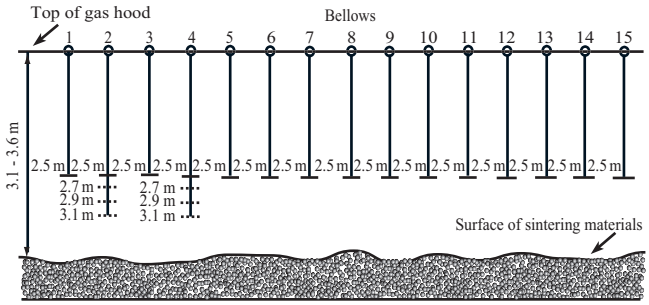

Fig. 5. Positions of thermocouples above bellows (= hood distances) for measurements on group containing Bellows 2 and 4.

Table 2. Measured gas temperatures for Bellows 2 and 4.

Measured gas temperature for Bellows 2 and 4 (°C)	Measured gas temperature (°C)			
	$T_1(2.5)$	$T_3(2.5)$	$T_5(2.5)$	$T_6(2.5)$
$T_2(2.7) = 137,\ T_4(2.7) = 187$	79	178	356	423
$T_2(2.9) = 131,\ T_4(2.9) = 180$	93	192	419	490
$T_2(3.1) = 124,\ T_4(3.1) = 190$	88	191	352	420

At a hood distance of 2.7 m, the measured gas temperature for Bellows 2 is $T_2(2.7) = 137°\text{C}$. At a hood distance of 2.5 m, the measured gas temperatures for Bellows 1, 3, 5, and 6 are $T_1(2.5) = 79°\text{C}$, $T_3(2.5) = 178°\text{C}$, $T_5(2.5) = 356°\text{C}$ and $T_6(2.5) = 423°\text{C}$, respectively. Using (1) to compute the gas temperature for Bellows 2 at a hood distance of 2.5 m yields $\hat{T}_2(2.5) = 161.83°\text{C}$. The difference in gas temperature and the relative change in gas temperature (RCGT) are

$$\begin{aligned}\Delta\hat{T}_2(2.5 \to 2.7) &= T_2(2.7) - \hat{T}_2(2.5) \\ &= 137°\text{C} - 161.83°\text{C} = -24.83°\text{C},\end{aligned} \tag{3}$$

$$\eta_{T_2}(2.5 \to 2.7) := \frac{\Delta\hat{T}_2(2.5 \to 2.7)}{\hat{T}_2(2.5)} \times 100\% = -15\%. \tag{4}$$

Similarly, at a hood distance of 2.9 m, the difference in gas temperature and the RCGT are

$$\begin{aligned}\Delta\hat{T}_2(2.5 \to 2.9) &= T_2(2.9) - \hat{T}_2(2.5) \\ &= 131\,°\text{C} - 189.52°\text{C} = -58.52°\text{C},\end{aligned} \tag{5}$$

$$\eta_{T_2}(2.5 \to 2.9) := \frac{\Delta\hat{T}_2(2.5 \to 2.9)}{\hat{T}_2(2.5)} \times 100\% = -31\%. \tag{6}$$

And at a hood distance of 3.1 m, the difference in gas temperature and the RCGT are

$$\begin{aligned}\Delta\hat{T}_2(2.5 \to 3.1) &= T_2(3.1) - \hat{T}_2(2.5) \\ &= 124°\text{C} - 185.42°\text{C} = -61.42°\text{C},\end{aligned} \tag{7}$$

$$\eta_{T_2}(2.5 \to 3.1) := \frac{\Delta\hat{T}_2(2.5 \to 3.1)}{\hat{T}_2(2.5)} \times 100\% = -33\%. \tag{8}$$

In like manner, the GTD for Bellows 4 is derived. After many experiments, the average RCGT at the measurement points was obtained, as shown in Table 3.

3.5 Model of Surface Temperature of Material

Based on the GTD obtained above, the temperature at any hood distance is given by

$$\begin{aligned}\hat{T}_i(h) = T_i(2.5) \times [1 + \eta_{T_i}(2.5 \to h)], \\ i = 1, \cdots, 15;\ h = 2.7, 2.9, 3.1.\end{aligned} \tag{9}$$

Table 3. Average RCGT at measurement points.

	Hood distance of Bellows 2 (m)			Hood distance of Bellows 4 (m)		
	2.7	2.9	3.1	2.7	2.9	3.1
Average RCGT	−14%	−30%	−32%	−30%	−33%	−31%

In the calculations, the average RCGT for Bellows 1 is taken to be that for Bellows 2. The average RCGT for Bellows 3 is calculated by taking the mean of the RCGTs for Bellows 2 and 4. The average RCGTs for Bellows 12-15 are taken to be that for Bellows 11. Table 4 shows the gas temperatures above the bellows of the sintering machine based on a set of production data.

Table 4 shows that the temperature measured closest to the surface of the material is not the highest, and that there are large temperature changes above Bellows 5, 6, and 7. The model of the surface temperature of the material is

$$\hat{T}_i(3.1) := T_i(2.5) \times [1 + \eta_{T_i}(2.5 \to 3.1)]. \tag{10}$$

4. DETERMINATION OF BTP BY SOFT-SENSING TECHNIQUE

Since the surface temperature of the material is close to the gas temperature at a hood distance of 3.1 m, the gas temperature at that distance is taken to be the approximate temperature of the surface. It is plotted in Fig. 6 for all the bellows.

Clearly, the part of the curve containing the highest point can be approximated by the following quadratic equation:

$$T = K_2 x^2 + K_1 x + K_0, \tag{11}$$

where T is gas temperature; x is the number of the bellows; and K_0, K_1, and K_2 are coefficients. Note that the highest point is one of the three points, $A(x_A, T_A(3.1))$, $B(x_B, T_B(3.1))$, or $C(x_C, T_C(3.1))$.

Let x_{BTP} be the BTP. Since the derivative of T with respect to x is zero when T is a maximum,

$$dT/dx = 2K_2 x_{\mathrm{BTP}} + K_1 = 0. \tag{12}$$

Thus,

Table 4. Gas temperatures above bellows of sintering machine.

Bellows	Hood distance (m)			
	2.5	2.7	2.9	3.1
1	84°C	72°C	59°C	57°C
2	194°C	166°C	136°C	132°C
3	208°C	162°C	142°C	142°C
4	268°C	188°C	180°C	185°C
5	453°C	371°C	417°C	282°C
6	512°C	476°C	463°C	370°C
7	587°C	540°C	559°C	527°C
8	633°C	655°C	550°C	554°C
9	694°C	741°C	553°C	595°C
10	734°C	662°C	730°C	680°C
11	706°C	655°C	568°C	620°C
12	684°C	634°C	550°C	577°C
13	653°C	606°C	525°C	550°C
14	610°C	566°C	490°C	514°C
15	587°C	545°C	472°C	495°C

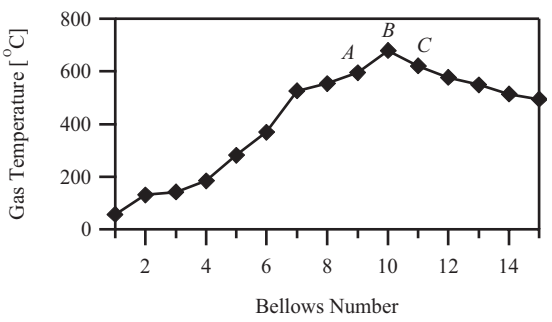

Fig. 6. Determination of BTP based on GTD.

$$x_{\mathrm{BTP}} = -K_1/(2K_2). \tag{13}$$

Bellows 1-14 are all 3 m long; so based on the model of surface temperature in Subsection 3.5, the actual position of the current BTP is $3x_{\mathrm{BTP}}$ m. The BTP is determined every three minutes.

5. INTELLIGENT INTEGRATED MODEL FOR PREDICTING BTP

This section explains how a BPNN is used to predict the BTP in the LZSP.

5.1 Time-Sequence-Based Grey Prediction Model

In order to control the BTP, a model for predicting the BTP must first be established. So, we built a time-sequence-based prediction model (TSBPM) for the BTP based on grey theory (Kung et al. [2007]).

The data on the BTP obtained in Section 4 is treated as the original sequence, $X^{(0)}(k)$, for the grey model, GM(1,1). That sequence is

$$X^{(0)}(k) = \left\{x^{(0)}(1),\ x^{(0)}(2),\ \cdots,\ x^{(0)}(n)\right\}, \tag{14}$$

where k is an observation index ($k = 1, 2, \cdots, n$).

Carrying out the accumulated generating operation (AGO)

$$x^{(1)}(k) = \sum_{i=1}^{k} x^{(0)}(i), \tag{15}$$

we obtain the accumulated sequence

$$X^{(1)}(k) = \left\{x^{(1)}(1),\ x^{(1)}(2),\ \cdots,\ x^{(1)}(n)\right\}. \tag{16}$$

The AGO reduces the variations in the original data, and is governed by an exponential-increase law. The whitened first-order differential equation is

$$\frac{dx^{(1)}}{dt} + ax^{(1)} = u, \tag{17}$$

where u is the grey input, and a is a development coefficient. They are determined by the least-squares method:

$$\hat{a} = [a \quad u]^T = (B^T B)^{-1} B^T Y, \tag{18}$$

where Y and B are

$$Y = \left[x^{(0)}(2),\ x^{(0)}(3),\ x^{(0)}(4),\ \cdots,\ x^{(0)}(n)\right]^T \tag{19}$$

and

$$B = \begin{bmatrix} -0.5\left\{x^{(1)}(1)+x^{(1)}(2)\right\} & 1 \\ -0.5\left\{x^{(1)}(2)+x^{(1)}(3)\right\} & 1 \\ -0.5\left\{x^{(1)}(3)+x^{(1)}(4)\right\} & 1 \\ \vdots & \vdots \\ -0.5\left\{x^{(1)}(n-1)+x^{(1)}(n)\right\} & 1 \end{bmatrix}. \quad (20)$$

GM(1,1) is

$$\hat{x}^{(1)}(k+1)=\left[x^{(0)}(1)-\frac{u}{a}\right]e^{-ak}+\frac{u}{a},\ k=0,1,\cdots,n. \quad (21)$$

The original sequence is converted to a real value by the following subtraction rule:

$$\hat{x}^{(0)}(1) = x^{(0)}(1), \quad (22)$$

$$\hat{x}^{(0)}(k+1)=x^{(1)}(k+1)-x^{(1)}(k),\ k=1,2,\cdots,n. \quad (23)$$

Thus, the TSBPM of the BTP is

$$\hat{x}_{\mathrm{BTP}_a}(k+1) = \left[x^{(0)}(1)-\frac{u}{a}\right]\left[e^{-ak}-e^{-a(k-1)}\right]. \quad (24)$$

5.2 Technological-Parameter-Based NN Prediction Model

Since the main factors affecting the BTP are the permeability of the material (P_e) and the trolley velocity (V), we establish a technological-parameter-based prediction model (TPBPM) to suppress variations in the state of the process.

First, we define permeability. Since sintering is completed before Bellows 10, the permeability of the LZSP is

$$P_e = \sum_{i=1}^{2} 0.075P_{ei} + \sum_{i=3}^{5} 0.15P_{ei} + \sum_{i=6}^{9} 0.1P_{ei}. \quad (25)$$

where P_{ei} is computed using the Voice formula (Zhou & Kong [1989]).

A BPNN with a three-layer structure (2-8-1) is employed to predict the BTP. The inputs are P_e and V; and the output is the BTP, $\hat{x}_{\mathrm{BTP}_b}(k+1)$. Regarding the number of hidden neurons, experiments have shown the prediction accuracy of the model to be satisfactory when the number is 8.

The TPBPM of the BTP is given by

$$\hat{x}_{\mathrm{BTP}_b}(k+1)=\sum_{i=1}^{8}\omega_{Oi}\mathrm{tansig}\left(\sum_{j=1}^{2}\omega_{ij}x_j+b_i\right)+b_O. \quad (26)$$

Moreover, a BP algorithm is used to train this NN. 1000 sets of qualified samples were used for modeling and verification. The initial weights and biases were in the range $[-1,1]$. Trial learning results showed the learning rate to be 0.2.

5.3 Integrated Model for Predicting BTP

Regarding the prediction of the BTP, the TSBPM has a high precision; but a large error arises when the parameters vary. The TPBPM can suppress these timewise variations, but that affects the prediction accuracy. So, the two prediction models are integrated using a fuzzy classifier into an integrated model for predicting the BTP.

Let ΔP_e and ΔV be the changes in P_e and V, respectively; and let $\mu(x)$ $(0 \le \mu(x) \le 1)$ be a technological-parameter-variation index. ΔP_e and ΔV are grouped using fuzzy classification, and $\mu(x)$ is defined to be

$$\mu(x) = \min\left\{\mu_{p_e}(\Delta P_e), \mu_V(\Delta V)\right\}. \quad (27)$$

Combining the above models yields the following integrated model for predicting the BTP:

$$\hat{x}_{\mathrm{BTP}}(k+1) = [1-\mu(x)]\hat{x}_{\mathrm{BTP}_a}(k+1) + \mu(x)\hat{x}_{\mathrm{BTP}_b}(k+1). \quad (28)$$

6. RESULTS OF ACTUAL RUNS

The intelligent integrated model described above was used to determine and predict the BTP in a nonferrous metal smeltery. The μXL distributed control system and management information system used previously, together with an industrial control computer, constitute a new optimization and control system (OCS) for the process. The OCS runs under the Windows operating system. The data communication software and application software were written in the C++ language. The BTP is predicted every three minutes; and the training of the NNs employs a BP algorithm that satisfies the requirements of real-time control.

Data from actual runs were used to verify both individual prediction models and the integrated one. In order to compare them, 101 sets of qualified samples were used to predict the BTP. The results of actual runs are shown in Figs. 7-9. In this system, a prediction is considered wrong if it is not within the range required by the technology. And the prediction error is defined to be the percentage of wrong predictions.

The results of actual runs show that the accuracy is 75.5% for the TSBPM, 82.5% for the TPBPM, and 89.5% for the integrated prediction model. Clearly, the integrated prediction model provides the highest accuracy. Maintenance on the integrated model is carried out once every year to verify that it is adapting appropriately. This OCS has been running well up to the present.

Statistical results for a year-long run of the OCS show the variation in the BTP to be 6.4%, while it was 12.4% for the old system. Thus, the new OCS reduces the variation by 50%, greatly improving the control accuracy. Clearly, the OCS, which employs the integrated model for predicting BTP, effectively suppresses variations in the BTP and stabilizes the quantity and quality of sintering agglomerate. It is also worth mentioning that a questionnaire on the OCS revealed that it greatly reduces the work load on the operators, and that the graphical user interface was designed to be user-friendly and easy to use.

7. CONCLUSIONS

Based on an analysis of the LZSP of a nonferrous metal smeltery, an integrated model for predicting the BTP was developed. The main points of the study are as follows:

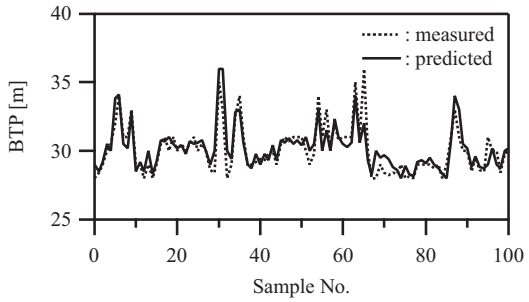

Fig. 7. Results of runs of TSBPM.

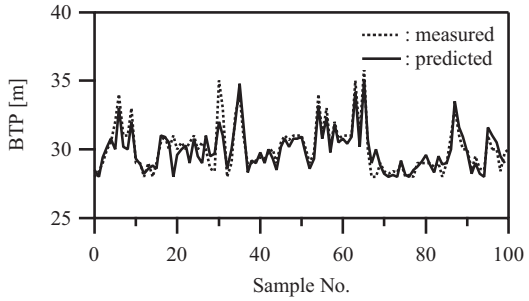

Fig. 8. Results of runs of TPBPM.

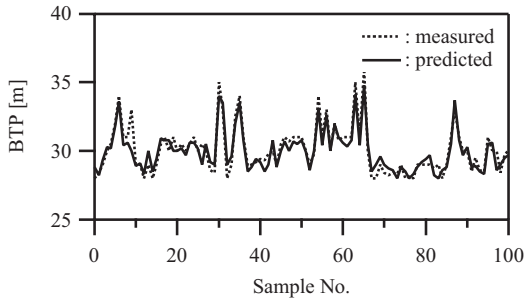

Fig. 9. Results of runs of integrated prediction model.

- The GTD of a sintering machine was investigated. NNs were used to obtain the features of the GTD, and a model of the surface temperature of the material was established.
- The model is used in combination with a soft-sensing technique to obtain the current BTP.
- A TSBPM of the BTP was built using grey theory and the model of the current BTP, and a TPBPM of the BTP was set up using an NN. Based on the idea of intelligent integration, a fuzzy classifier was employed to make an integrated model for predicting the BTP so as to guarantee a high prediction accuracy.
- The results of actual runs show that the accuracy of the integrated prediction model is 89.5%. After an optimization and control system was put into operation, the variation in the BTP was reduced by about 50%, thus effectively stabilizing the LZSP.

ACKNOWLEDGEMENTS

The authors would like to thank Prof. Wei-Hua Cao of Central South University, Dr. Yu-Xiao Du of Guangdong University of Technology, and Engineers Xian-De Zhou and Xiong-Qi Shao of Shaoguan Smeltery for their contributions to this project.

REFERENCES

E. Jak, B.J. Zhao, I. Harvey, and P.C Hayes. Experimental study of phase equilibria in the PbO-ZnO-"Fe_2O_3" - ($CaO + SiO_2$) system in air for the lead and zinc blast furnace sinters (CaO/SiO_2 weight ratio of 0.933 and $PbO/(CaO + SiO_2)$ ratios of 2.0 and 3.2). *Metallurgical and Materials Transactions B: Process Metallurgy and Materials Processing Science*, volume 34, 4: 383–397, 2003.

J.R. Siemon, E. Kowalczyk, D.P. Fitzgibbons, and W. Baguley. Peak bed temperature prediction on a lead/zinc sinter plant. *Minerals Engineering*, volume 4, 1: 63–78, 1991.

M.H. Li and Y.F. Sun. Study of the fuzzy control system for burning through point of sintering. *Journal of Huazhong University of Science and Technology*, volume 32, 4: 71–73, 2004.

J. Terpak, L. Dorcak, I. Kostial, and L. Pivka. Control of burn-through point for agglomeration belt. *Metalurgija*, volume 44, 4: 281–284, 2005.

X.H. Yuan and H. He. Neural network model of burn through point temperature and ventilating index algorithm for sintering system. *Computer Engineering and Design*, volume 27, 6: 1028–1029, 2006.

W.H. Kwon, Y.H. Kim, S.J. Lee, and K.N. Paek. Event-based modeling and control for the burning through point in sintering processes. *IEEE Transaction on Control System Technology*, volume 7, 1: 31–41, 1999.

Er.M. Joo, J. Liao, and J.Y. Lin. Fuzzy neural networks-based quality prediction system for sintering process. *IEEE Transaction on Fuzzy Systems*, volume 8, 3: 314–324, 2000.

M. Wu, J.H. She, and M. Nakano. An expert control system using neural networks for the electrolytic process in Zinc hydrometallurgy. *Engineering Applications of Artificial Intelligence*, volume 14, 5: 589–598, 2001.

C.H. Yang, G. Deconinck, W.H. Gui, and Y.G. Li. An optimal power-dispatching system using neural network for the electrochemical process of zinc depending on varying prices of electricity. *IEEE Transactions on Neural Networks*, volume 13, 1: 229–236, 2002.

X.R. Tang, D.Y. Wang, and Q.C. Zhang. *Sintering theory and technology.* Central South University of Technology Press, Changsha, 1992.

M.T. Hagan, H.B. Demuth, and M.H. Beale. *Neural network design.* China Machine Press, Beijing, 2002.

C.Y. Kung and K.L. Wen. Applying grey relational analysis and grey decision-making to evaluate the relationship between company attributes and its financial performance–a case study of venture capital enterprises in Taiwan. *Decision Support Systems*, volume 43, 3: 842–852, 2007.

Q.D. Zhou and L.T. Kong. *The theory and technology of iron ore agglomeration.* Metallurgical Industry Press, Beijing, 1989.